

Indirect Sliding Mode Power Control associated to Virtual-Resistor-based Active Damping Method for *LLCL*-Filter-based Grid-Connected Converters

M. Ben Saïd-Romdhane*, M. W. Naouar**, I. Slama-Belkhodja***, E. Monmasson****

*****Université de Tunis El Manar, Ecole Nationale d'Ingénieurs de Tunis, LR 11 ES 15, Laboratoire des Systèmes Electriques, BP 37-1002, Tunis le Belvédère, Tunisie.

****SATIE, University of Cergy-Pontoise, 33 bd du Port, 95000 Cergy-Pontoise, France.

Received: 14.01.2017 Accepted:03.04.2017

Abstract- *LLCL* filters are becoming an attractive solution for Grid connected Converters (GcCs) due to their ability to reduce the filter cost and size while meeting new grid codes and power quality requirements. Compared to the conventional *LCL* filter, the *LLCL* filter introduces an additional inductor in the capacitor branch to form a series *LC* circuit that resonates at the GcC switching frequency. The *LC* branch has a low impedance at the switching frequency, which can greatly eliminate the harmonic current and therefore reduce the filter grid side inductor. However, the *LLCL* filter resonance phenomenon and the large changes in the grid inductance (typically under weak grid conditions and in rural areas) may compromise the system stability. In order to address these concerns, this paper proposes an Indirect Sliding Mode Power Control associated to Virtual Resistor based Active Damping method (ISMPC-VRAD) for *LLCL*-filter-based Grid-connected Converters (*LLCL*-GcCs). The *LLCL* filter design parameters as well as the ISMPC-VRAD gains are carefully tuned in order to ensure stable operation under severe grid inductance variations while taking into account the influence of *LLCL* filter parameters changes on the system stability. Simulation results are presented and discussed in order to prove the efficiency and the reliability of the proposed ISMPC-VRAD for *LLCL*-GcCs as well as high filtering performances of the designed *LLCL*-GcCs.

Keywords *LLCL* filter, Grid connected Converters (GcCs), Indirect Sliding Mode Power Control (ISMPC), Virtual Resistor based Active Damping method (VRAD), large grid impedance variation.

Nomenclature

AD	Active Damping	L_s^g	sum of filter filter side inductance and grid inductance
GcC	Grid connected Converter	P	active power
$ISMPC$	Indirect Sliding Mode Power Control	P_n	rated active power
$LLCL-GcC$	<i>LLCL</i> -filter-based Grid-connected Converters	Q	reactive power
PCC	Point of common coupling	Q_c	reactive power consumed by the filter capacitor <i>LLCL</i> filter
PD	Passive Damping	R_{ch}	resistive load
THD	Total Harmonic Distortion	R_d	damping resistance
$VRAD$	Virtual Resistor based Active Damping method	$S_{i(a,b,c)}$	switching states of the converter (for $k=a,b,c$ phases)
SVM	Space Vector Modulation	S_{2dq}	switching functions
C_f	<i>LLCL</i> filter capacitance	\dot{S}_{2dq}	time derivatives of the switching functions
f_g	rated frequency of grid voltage	U_{gn}	line-to-line RMS grid voltage
f_{res}	resonance frequency of <i>LLCL</i> filter	$V_{c(a,b,c)}$	voltage across the filter capacitor in series with the damping resistor (for $k=a,b,c$ phases)
f_{sw}	switching frequency of the power converter	V'_c	voltage across the filter capacitor
$i_{c(a,b,c)}$	<i>LLCL</i> filter capacitor current (for $k=a,b,c$ phases)	V_{dc}	voltage of power converter capacitor
i_{dq}	<i>dq</i> -axis current of <i>dq</i> transformation	V_{dq}	<i>dq</i> -axis voltage of <i>dq</i> transformation
$i_{i(a,b,c)}$	converter side current (for $k=a,b,c$ phases)	V_{dq}^{att}	attractive voltage vector
i_{in}	n harmonic order of the converter side current	V_{dq}^{eq}	equivalent voltage vector
i_{2n}	n harmonic order of the grid side current	$V_{g(a,b,c)}$	grid voltage (for $k=a,b,c$ phases)
I_{sat}	saturation current of the <i>LCLL</i> filter inductors	$V_{i(a,b,c)}$	power converter output voltage (for $k=a,b,c$ phases)
i_{sw}	switching frequency harmonic order of the current	V_{in}	n harmonic order of the converter side voltage
$i_{2(a,b,c)}$	grid side current (for $k=a,b,c$ phases)	V^*	reference voltage
i^*	reference current	θ_{dq}	grid voltage vector phase
K_r	virtual resistor	δ	harmonic attenuation rate
L_f	trap inductance of the <i>LLCL</i> filter	Δ_{imax}	maximum converter current ripple
L_g	inductive part of the grid impedance	ω_g	rated angular frequency of the grid voltage
L_i	<i>LLCL</i> filter converter side inductance	ω_{res}	resonance angular frequency of the filter
L_T	<i>LLCL</i> filter total inductance	ω_{sw}	switching angular frequency of the converter
L_2	<i>LLCL</i> filter grid side inductance		

1. Introduction

In order to meet new grid codes and their on-going changes in the near future, Grid-connected Converters (GcCs) employ a passive low-pass filter for connection with the grid. The introduced filter can be either an *L* filter (Fig.1.a), an *LCL* filter (Fig.1.b), an *LLCL* filter (Fig.1.c) or a multi-tuned filter (Fig.1.d). Despite being simple, the *L* filter has bulky size (large inductance value) and low harmonic attenuation characteristic. Compared with *L* filter, the *LCL* filter is a third order system able to reduce significantly switching harmonic injection as well as filter cost and encumbrance [1][2][3]. The required inductor and capacitor values can further be reduced by replacing the capacitor branch of an *LCL* filter with a series *LC* trap, as shown in Fig.1.c. The resulting filter is named *LLCL* filter [4]. Compared to the *LCL* filter, the *LLCL* filter has an extra small inductor L_f added in series with the filter capacitor. This inductor, together with the capacitor C_f , is

tuned to resonate at the GcC switching frequency. Harmonics around the switching frequency will then flow through the low impedance path composed by L_f and C_f , rather than their injection into the grid. Hence, the *LLCL* filter can attenuate the switching frequency harmonics better than the *L* and the *LCL* filters while reducing the total inductor value and size [5][6]. The same principle can be repeated by introducing more *LC* traps designed at other dominant harmonic frequencies (such as $2f_{sw}$, $3f_{sw}$...), as shown in Fig.1.d [6][7]. Due to the complexity introduced by this filter, the number of trap is kept at one and the selected passive low-pass filter is the fourth order *LLCL* filter. However, closed loop current control of *LLCL*-filter-based Grid-connected Converter (*LLCL-GcC*) may be unstable because of the related resonance problem. Consequently, robust current control strategies are required to maintain system stability.

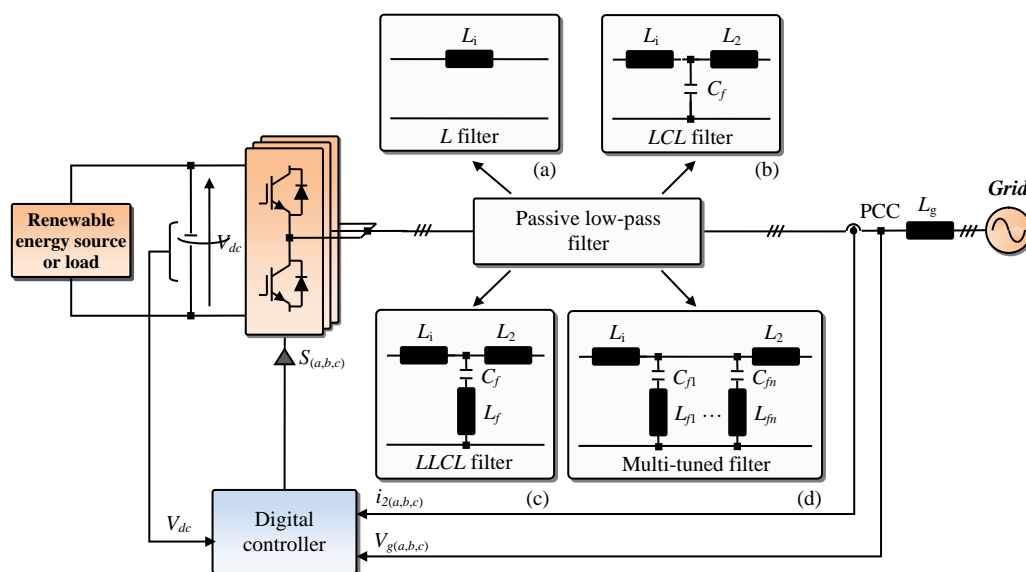


Fig. 1. (a) Power circuit of the GcC with (a) *L* filter (b) *LCL* filter (c) *LLCL* filter (d) multi-tuned filter

Several standard control strategies with constant switching frequency have been developed in literature. The most used ones are the voltage-oriented PI control (VOC) [8][9], the Direct Power Control associated to the Space Vector Modulator (DPC-SVM) [10] and the Indirect Sliding Mode Power Control (ISMPC) [11][12]. Compared to the VOC and the DPC-SVM control strategies, the ISMPC is characterized by low current Total Harmonic Distortion (THD) factor, fast transient response, non-use of integral terms as well as robustness against external disturbances and parameters variations [12]. However, due to the inherent resonance phenomenon of *LLCL* filters, the stability region of the ISMPC is limited. Similarly to the *LCL* filter, passive damping method (PD), achieved by introducing a resistor in series with the filter capacitor, is the simplest solution to damp the *LLCL* filter resonance [13]. However, this method has several drawbacks, such as reduced system efficiency and power losses [14]. Instead of PD methods, the active damping

(AD) ones, obtained by modifying the control algorithm without using dissipative elements, have been also suggested for *LLCL-GcCs*. The AD methods are based either on a digital filter (such as a Notch filter [15][16], a lead-lag compensator [17] or quite simply a low-pass filter [18]) or a multi-loop control (such as filter capacitor current inner loop [19][20] and Virtual Resistor based Active Damping (VRAD) [21][22]). The filter based AD methods have the benefit of reducing the sensors number, but they are more sensitive to parameters variations and disturbances. It should be noted that, in most current research works, the PD and AD methods for high order filter based GcCs (such as *LCL-GcCs* and *LLCL-GcCs*) are associated only to VOC control strategy.

Depending on the grid conditions (weak or stiff grid) [23][24] and configuration (low, medium or high voltage lines, wires length...) [25][26], the grid impedance variations can weaken the damping effect and challenge the control of *LLCL-GcCs* in terms of stability. In this context, the aim of

this paper is to propose an Indirect Sliding Mode Power Control associated to Virtual Resistor based Active Damping method (ISMPC-VRAD) for the *LLCL-GcC*. The *LLCL* filter design parameters as well as the ISMPC-VRAD gains are carefully tuned in order to ensure stable operation under severe grid inductance variations while taking into account the influence of *LLCL* filter parameters changes on the system stability. To summarize, compared to previous related works, the new features of this paper are: 1) The association between robust control strategy (ISMPC) and robust active damping method (VRAD); 2) robustness against large grid inductance variations, overestimated to 13 mH; 3) robustness against filter parameters variations, overestimated to $\pm 20\%$; 4) a simple and systematic method for the tuning of the ISMPC-VRAD gains in order to ensure simultaneously a low harmonic attenuation rate δ and a grid current THD value less than 5%.

This paper is organized as follows. Firstly, in section 2, the mathematical model and the parameters design of the *LLCL-GcC* are presented. Then, in section 3, the stability analysis of the ISMPC-VRAD for *LLCL-GcC* is detailed and discussed. Then, in section 4, the theoretical analysis of Section 3 was verified through simulation results achieved under Matlab-Simulink software tool. The obtained simulation results prove performances, effectiveness and robustness of the proposed ISMPC-VRAD algorithm as well as high filtering performances of the designed *LLCL-GcC*.

2. LLCL filter mathematical model and parameters design

2.1. Mathematical model

Assuming that the grid three phases system is balanced, the equivalent single phase representation of an *LLCL-GcC* power circuit is given by Fig.2.

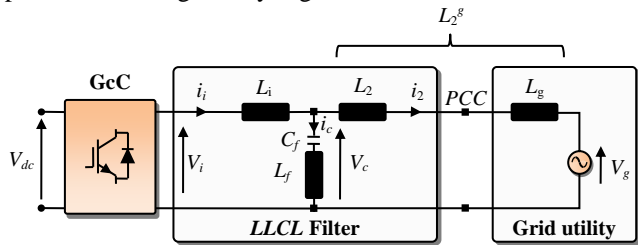


Fig. 2. Single phase equivalent circuit of *LLCL-GcC*

According to this figure, the *LLCL* filter equations can be expressed as follows

$$\begin{aligned}
 i_i &= \frac{V_i - V_c}{L_f s} & (a) & & i_2 &= \frac{V_c - V_g}{L_2^g s} & (b) \\
 V_c &= \left(\frac{1}{C_f s} + L_f s\right) i_c & (c) & & i_c &= i_i - i_2 & (d)
 \end{aligned}
 \tag{1}$$

By applying the *abc-to-dq* coordinate transformation to equations given by (1) and neglecting the decoupling terms between the *d* and *q* axes, the simplified block diagram of an *LLCL-GcC* power circuit in the *dq* frame (where the *d*-axis is linked to the grid voltage vector) is depicted on Fig.3.

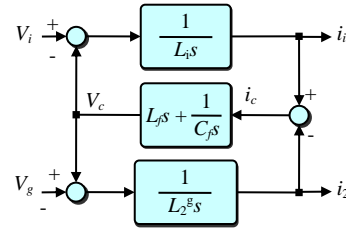


Fig. 3. Simplified *dq*-axis *LLCL-GcC* block diagram

Assuming that the grid voltage is an ideal sine wave, the high frequency *LLCL-GcC* transfer function F_1 is expressed by equation (2). Based on this equation, the *LLCL-GcC* resonance frequency (that corresponds to zero impedance) is given by (3). The transfer function between i_{in} and V_{in} (for high frequencies) can be approximated as in (4) [27]. Based on equations (2) and (4), the high frequency transfer function between the grid and the converter currents is expressed by equation (5). At the switching frequency, the previous equation becomes equal to (6).

$$F_1 = \frac{i_{2n}}{V_{in}} = \frac{C_f L_f s^2 + 1}{C_f (L_f (L_i + L_2^g) + L_i L_2^g) s^3 + (L_i + L_2^g) s} \tag{2}$$

$$f_{res} = \frac{1}{2\pi} \sqrt{\frac{L_i + L_2^g}{L_i L_2^g C_f + (L_i + L_2^g) L_f C_f}} \tag{3}$$

$$\frac{i_{in}}{V_{in}} = \frac{1}{L_i s} \tag{4}$$

$$\frac{i_{2n}}{i_{in}} = \frac{L_i (C_f L_f s^2 + 1)}{C_f (L_f (L_i + L_2^g) + L_i L_2^g) s^2 + (L_i + L_2^g)} \tag{5}$$

$$\left| \frac{i_{2s\omega}}{i_{is\omega}} \right| = \left| \frac{L_i (C_f L_f \omega_{s\omega}^2 + 1)}{C_f (L_f (L_i + L_2^g) + L_i L_2^g) \omega_{s\omega}^2 + (L_i + L_2^g)} \right| \tag{6}$$

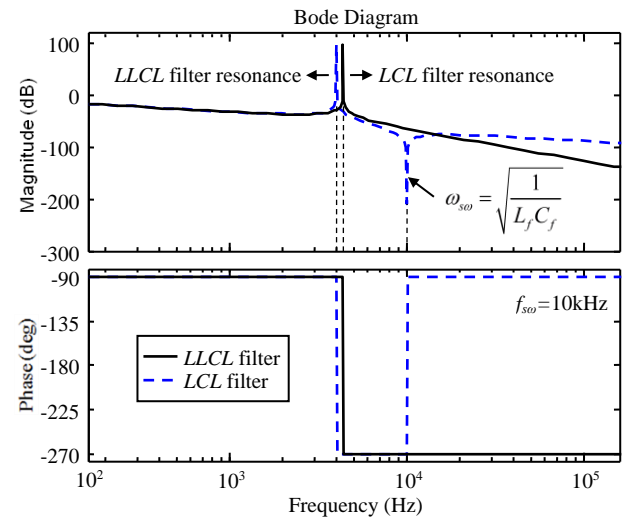


Fig. 4. Bode diagram of F_1 in case of *LLCL* and *LCL* filters

Fig.4 shows the Bode diagram of the transfer function F_1 of both the *LLCL* filter and the *LCL* filter (F_1 with L_f is set to zero). In this figure, the parameters of the *LLCL* and *LCL* filters are the same except for the L_f . This figure shows that

the *LCL* and *LLCL* filters have the same frequency response in the frequency range lower than the filter resonance frequency. Although, it exists a low impedance in the *LLCL* filter at the switching frequency. This negative impedance is caused by the *LC* branch and offers to the *LLCL* filter higher harmonic attenuation at the switching frequency compared to the *LCL* filter.

2.2. Parameters design

The design of an *LLCL* filter requires the following input data: U_{gn} , P_n , f_g , f_{sw} , V_{dc} and I_{sat} . The tuning of the *LLCL* filter parameters is detailed in the following steps.

- Step 1: Determination of f_{res} condition

Since the resonance frequency is a decreasing function of L_g variable (equation (3)), the range of resonance frequency variation is given by the following equation

$$f_{res\ min} \leq f_{res}(L_g) \leq f_{res\ max}$$

$$f_{res\ min} = \frac{1}{2\pi} \sqrt{\frac{L_i + L_{2\ max}^g}{L_i L_{2\ max}^g C_f + (L_i + L_{2\ max}^g) L_f C_f}} \quad (7)$$

$$f_{res\ max} = \frac{1}{2\pi} \sqrt{\frac{L_i + L_{2\ min}^g}{L_i L_{2\ min}^g C_f + (L_i + L_{2\ min}^g) L_f C_f}}$$

On the other hand and in order to avoid resonance problems, f_{res} must be higher than 10 times f_g and less than half of f_{sw} [9]. Consequently, in order to avoid system instability due to large grid impedance changes and resonance problems, the range of resonance frequency variation must verify the following condition

$$10f_g < f_{res\ min} \leq f_{res}(L_g) \leq f_{res\ max} < f_{sw}/2 \quad (8)$$

- Step 2: Tuning of $L_{T\ max}$

In order to reduce the voltage drops and the losses in the filter, the L_T value should be as small as possible. To this purpose, $L_{T\ max}$ should be lower than 0.1 pu as shown in equation (9) [27].

$$L_{T\ max} = 10\% \frac{U_{gn}^2}{2\pi f_g P_n} \quad (9)$$

- Step 3: Tuning of $C_{f\ max}$

Reactive power consumed by the filter capacitor Q_c should be constrained less than $\lambda\%$ of the rated power P_n in order to avoid power factor decrease as shown in equation (10). Based on this condition and for λ equal to 5 [9], the maximum filter capacitor value is given by (11). It should be noted that when the value of C_f is too low, the inductor values must be too high. Otherwise, if the value of C_f is too high, the inductor values will be smaller and therefore the current ripples become more important. To this purpose, it is advisable to begin with a capacitor value equal to one half of the maximum value. If some of the constraints are not verified, the capacitor value should be increased up to the maximum value.

$$|Q_c| = U_{gn}^2 C_f \omega_g \leq \lambda\% |P_n| \quad (10)$$

$$C_{f\ max} = 5\% \frac{P_n}{2\pi f_g U_{gn}^2} \quad (11)$$

- Step 4: Tuning of $L_{i\ min}$

The main objective of the converter side inductor L_i is to reduce the converter current ripple. The minimum value of L_i is given by equation (12.a) [27]. On the other hand, the converter side current i_i must verify equation (12.b) in order to avoid inductor saturation problems. Consequently, according to equations (12.a) and (12.b), $L_{i\ min}$ can be deduced based on equation (13).

$$L_{i\ min} = \frac{V_{dc}}{6f_{sw} \Delta i_{max}} \quad (a) \quad \left| I_{i\ max} + \frac{\Delta i_{max}}{2} \right| < I_{sat} \quad (b) \quad (12)$$

$$L_{i\ min} > \frac{V_{dc}}{12f_{sw} (I_{sat} - I_{i\ max})} \quad (13)$$

Where $I_{i\ max} = I_{2\ max}$ (for high frequencies).

- Step 5: Tuning of L_f

In order to ensure zero impedance at the switching frequency, the value of the inductor in series with the filter capacitor L_f is computed according to the following equation

$$L_f = \frac{1}{C_f (2\pi f_{sw})^2} \quad (14)$$

- Step 6: Tuning of L_2

The main objective of the grid side inductor L_2 is to reduce the grid current harmonics according to grid code requirements. Based on the IEEE 519-1992 standard, the value of the grid current THD should be less than 5% [28]. The relation between L_2 and L_i is given by equations (15.a).

$$L_2 = aL_i \quad (a) \quad \text{where} \quad 0 \leq a \leq a_{max}$$

$$\text{and} \quad a_{max} = \frac{L_{T\ max}}{L_i} - 1 \quad (b) \quad (15)$$

By substituting L_2 by its expression given by equation (15.a), equation (6) becomes equal to equation (16) (for L_g equal to zero). In equation (16), δ is the harmonic attenuation rate. It is the ratio between the converter and the grid currents at the switching frequency. The positive solution of equation (16) is given by equation (17). Based on equations (15.a) and (17), L_2 can be expressed as in equation (18).

$$\delta = \frac{|i_{2\ sw}|}{|i_{isw}|} = \frac{C_f L_i b \omega_{sw}^2 + 1}{|(1+a)(C_f L_i b \omega_{sw}^2) + C_f L_i a \omega_{sw}^2|} \quad (16)$$

$$a = \frac{a_2 - \delta a_2}{\delta a_3} \quad (17)$$

$$L_2 = \frac{L_i a_2 (1 - \delta)}{\delta a_3} \quad (18)$$

Where $a_2 = 1 + C_f L_f \omega_{sw}^2$ and $a_3 = 1 + C_f \omega_{sw}^2 (L_f + L_i)$. By substituting L_2 by its expression given by equation (18), $f_{res\ min}$ and $f_{res\ max}$ (expressed by equation (7)) are given by equations (19) and (20), respectively.

$$f_{res\ min} = \frac{1}{2\pi} \sqrt{\frac{\delta a_4 + L_i a_2}{\delta a_5 + a_0 a_2}} \quad (19)$$

$$f_{res\ max} = \frac{1}{2\pi} \sqrt{\frac{\delta b_4 + L_i a_2}{\delta b_5 + a_0 a_2}} \quad (20)$$

Where $a_1=L_i L_{gmin} C_f + L_f C_f (L_i + L_{gmin})$, $a_4=a_3(L_i + L_{gmin}) - a_2 L_i$, $a_5=a_1 a_3 - a_2 a_0$, $b_1=L_i L_{gmax} C_f + L_f C_f (L_i + L_{gmax})$, $b_5=b_1 a_3 - a_2 a_0$, $b_4=a_3(L_i + L_{gmax}) - a_2 L_i$ and $a_0=L_i C_f (L_i + L_f)$. According to equations (8), (19) and (20), δ must verify the conditions expressed respectively by equations (21) and (22) in order to ensure system stability even for large grid impedance variations and resonance problems. On the other hand, the desired harmonic attenuation rate must be greater than a minimum harmonic attenuation rate δ_{min} expressed by equation (23).

$$10f_g < f_{res\ min} = \frac{1}{2\pi} \sqrt{\frac{\delta a_4 + L_i a_2}{\delta a_5 + a_0 a_2}} \quad (21)$$

$$\Rightarrow \delta < \frac{a_2 L_i - a_0 a_2 (20\pi f_g)^2}{a_5 (20\pi f_g)^2 - a_4}$$

$$f_{res\ max} = \frac{1}{2\pi} \sqrt{\frac{\delta b_4 + L_i a_2}{\delta b_5 + a_0 a_2}} < f_{swo} / 2 \quad (22)$$

$$\Rightarrow \delta < \frac{a_0 a_2 (\pi f_{swo})^2 - a_2 L_i}{b_4 - b_5 (\pi f_{swo})^2}$$

$$\delta > \delta_{min} = \frac{C_f L_f \omega_{swo}^2 + 1}{(1 + a_{max})(C_f L_f \omega_{swo}^2) + C_f L_i a_{max} \omega_{swo}^2} \quad (23)$$

The desired harmonic attenuation rate δ should be chosen according to equations (21), (22) and (23). Moreover, it shouldn't be too high since the harmonics are lower when δ is lower. In other words, when δ is lower, the obtained grid current THD value is lower. The selection of δ allows the determination of a based on equation (17). Then, the L_2 value is deduced according to equation (18).

- Step 7: Tuning of R_d

In order to avoid resonance problems, the simplest solution is to add a resistor in series with the filter capacitor. The added damping resistor R_d is computed according to equation (24). The power losses P_d associated to R_d are given by equation (25) [9]. In equation (25), λ is a positive constant selected so

that the power losses related to the damping resistor do not exceed 1% of the rated active power.

$$R_d = \frac{(Z_{LC})_{res}}{\lambda} = \frac{1}{\lambda} (2\pi f_{res} L_f + \frac{1}{2\pi f_{res} C_f}) \quad (24)$$

$$P_d = 3R_d \sum_n (i_{in} - i_{2n})^2 \quad (25)$$

The *LLCL* filter parameters design has been applied to a system with U_{gn} equal to 400V, P_n equal to 4kW, f_g equal to 50Hz, f_{swo} equal to 10kHz, V_{dc} equal to 600V and I_{sat} equal to 12A. Based on the design methodology presented and detailed in the previous paragraph, the current harmonic attenuation rate δ should be between 3.3% and 34%. A current harmonic attenuation rate δ equal to 7% is selected. Tab.1 summarizes the used system and the *LLCL* filter parameters.

Table 1. System and *LLCL* filter parameters

	Parameter	Value
System	U_{gn}	400V
	P_n	4kW
	f_{swo}	10kHz
	f_g	50Hz
	V_{dc}	600V
<i>LLCL</i> filter	L_i	5mH
	L_2	2mH
	C_f	4μF
	L_f	63.33μH
Damping resistor	R_d	6Ω
Grid inductance	L_g	$L_{gmin}=0mH$ and $L_{gmax}=13mH$

3. ISMPC-VRAD for *LLCL-GcC*

The performance of an *LLCL-GcC* depends not only on an appropriate design methodology of the filter, but also on an effective control strategy. This is due to the fact that the *LLCL* filter resonance phenomenon and the large changes in the grid inductance may compromise the system stability. Fig.4 shows the proposed robust ISMPC-VRAD for *LLCL-GcC*. It is made up of both an internal and external control loop. The internal one is based on the ISMPC-VRAD algorithm, while the external one is based on a PI controller that controls the dynamic and the shape of the dc-link voltage V_{dc} .

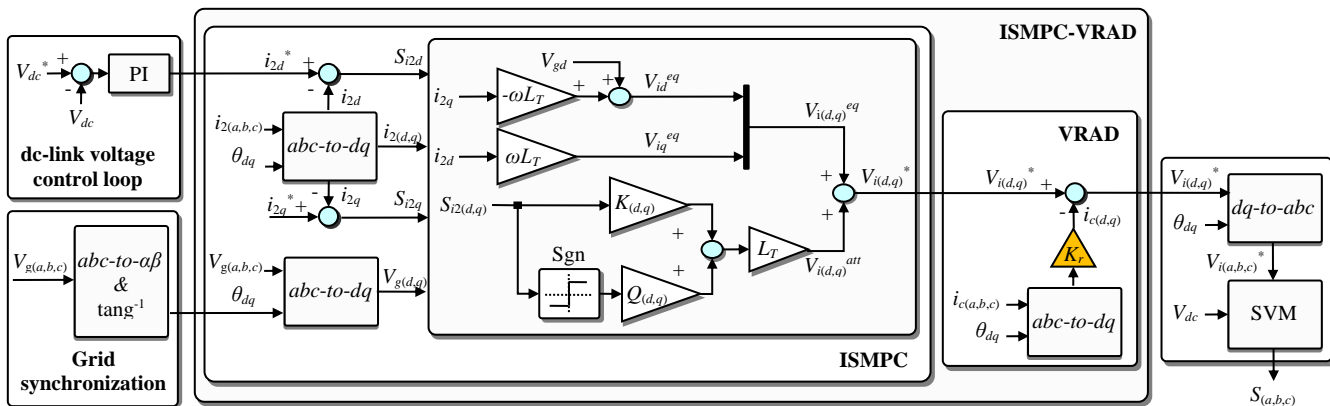


Fig. 5. ISMPC-VRAD for *LLCL-GcC*

The internal loop incorporates the ISMPC and the VRAD algorithms. The ISMPC algorithm controls the grid currents in the dq synchronous reference frame. The d -axis grid current reference i_{2d}^* is computed by the PI controller of the outer dc-link voltage control loop, whereas the q -axis grid current i_{2q}^* is set to zero in order to impose a unit power factor operation. The VRAD algorithm is used to actively damp the $LLCL$ filter resonance. As shown in this figure, it is achieved by sensing the capacitor current, multiplying it with a constant K_r and subtracting the result from the dq components $V_{i(d,q)}^*$ of the output power converter voltage vector. For such case, the constant K_r behaves like a real damping resistor in series with the filter capacitor without supplementary losses and encumbrance. Finally, the switching states $S_{(a,b,c)}$ of the converter are generated based on the SVM module. Note that the Park transformation (abc -to- dq) and the inverse Park transformation (dq -to- abc) are based on the position θ_{dq} of the grid voltage vector. The principle of the ISMPC algorithm is presented in the next paragraph.

3.1. Principle of ISMPC algorithm

For fundamental signals, the $LLCL$ filter can be approximated to an inductor with a value L_T equal to the sum of the two inductor values L_1 and L_2 [27]. Based on Fig.2 (for fundamental signals), the $LLCL$ - GcC filter equations in the dq reference frame are given by equations (26) and (27).

$$V_{id} = L_T \frac{di_{2d}}{dt} - \omega_g L_T i_{2q} + V_{gd} \quad (26)$$

$$V_{iq} = L_T \frac{di_{2q}}{dt} + \omega_g L_T i_{2d} \quad (27)$$

In case of ISMPC, the trajectory of the grid currents is made up of two modes as shown in Fig.6. The first one is the attractive mode. During this stage, the trajectory starts from a zero initial point and moves until it reaches the sliding surface at t_0 (during transient state). The second mode is the sliding mode. During this stage, the trajectory remains on the sliding surface (during steady state).

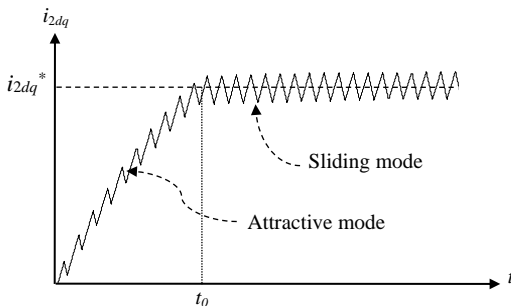


Fig. 6. Trajectory characterizing the ISMPC

The objective of the ISMPC is to control the active and reactive power through the control of i_{2d} and i_{2q} , respectively. To this purpose, S_{i2d} and S_{i2q} are defined as the difference between i_{2d}^* (respectively i_{2q}^*), and i_{2d} (respectively i_{2q}) as shown in equations (28) and (29), respectively. These

switching functions S_{i2d} and S_{i2q} define two sliding surfaces ($S_{i2d}=0$) and ($S_{i2q}=0$).

$$S_{i2d} = i_{2d}^* - i_{2d} \quad (28)$$

$$S_{i2q} = i_{2q}^* - i_{2q} \quad (29)$$

The ISMPC algorithm is synthesized so that the switching functions are attracted to their sliding surfaces during transient state (attractive mode). This means that the d and q grid side current components will be also attracted to their references. For this purpose, the switching functions (S_{i2d} and S_{i2q}) and their time derivatives must verify the following attractive conditions.

$$\dot{S}_{i2d} S_{i2d} < 0 \quad (30)$$

$$\dot{S}_{i2q} S_{i2q} < 0 \quad (31)$$

Once the sliding surfaces are reached, and in order to keep the switching functions on their sliding surfaces during steady state (sliding mode), the invariance conditions given by equations (32) and (33) must be verified.

$$S_{i2d} = 0 \quad \text{and} \quad \dot{S}_{i2d} = 0 \quad (32)$$

$$S_{i2q} = 0 \quad \text{and} \quad \dot{S}_{i2q} = 0 \quad (33)$$

The ISMPC-VRAD algorithm is executed at each sampling period T_e and between two consecutive sampling periods, the references i_{2d}^* and i_{2q}^* are constant. So, their time derivatives are null ($di_{2d}^*/dt=0$ and $di_{2q}^*/dt=0$). Consequently, based on equations (26), (27), (28) and (29), the time derivatives of the switching functions are expressed as follows

$$\dot{S}_{i2d} = -\frac{di_{2d}}{dt} = \frac{1}{L_T} (V_{gd} - \omega_g L_T i_{2q} - V_{id}) \quad (34)$$

$$\dot{S}_{i2q} = -\frac{di_{2q}}{dt} = \frac{1}{L_T} (\omega_g L_T i_{2d} - V_{iq}) \quad (35)$$

The computation of the reference voltage vector in the dq synchronous reference frame must be done so that the attractive and invariance conditions are satisfied. The reference voltage vector is composed of two terms as shown in equations (36) and (37). The first one (V_{id}^{att} and V_{iq}^{att}) ensures the control of the system during the attractive mode and it is active in the transient state. The second one (V_{id}^{eq} and V_{iq}^{eq}) ensures the control of the system during the sliding mode and it is active in the steady state.

$$V_{id}^* = V_{id}^{att} + V_{id}^{eq} \quad (36)$$

$$V_{iq}^* = V_{iq}^{att} + V_{iq}^{eq} \quad (37)$$

Based on equations (28), (29), (34) and (35), V_{id}^{eq} and V_{iq}^{eq} are deduced as in (38) and (39), respectively.

$$\begin{cases} S_{i2d} = 0 \\ \dot{S}_{i2d} = 0 \end{cases} \mapsto \begin{cases} i_{2d}^* = i_{2d} \\ \dot{S}_{i2d} = \frac{1}{L_T} (V_{gd} - \omega_g L_T i_{2q} - V_{id}^{eq}) = 0 \end{cases} \quad (38)$$

$$\mapsto V_{id}^{eq} = V_{gd} - \omega_g L_T i_{2q}$$

$$\begin{cases} S_{i2q} = 0 \\ \dot{S}_{i2q} = 0 \end{cases} \mapsto \begin{cases} i_{2q}^* = i_{i2q} \\ \dot{S}_{i2q} = \frac{1}{L_T} (\omega_g L_T i_{2d} - V_{iq}^{eq}) = 0 \end{cases} \quad (39)$$

$$\mapsto V_{iq}^{eq} = \omega_g L_T i_{2d}$$

According to equations (34), (35), (36), (37), (38) and (39), V_{id}^* and V_{iq}^* are expressed as follows

$$V_{id}^* = \underbrace{-L_T \frac{dS_{i2d}}{dt}}_{V_{id}^{att}} + \underbrace{V_{gd} - \omega L_T i_{2q}}_{V_{id}^{eq}} \quad (40)$$

$$V_{iq}^* = \underbrace{-L_T \frac{dS_{i2q}}{dt}}_{V_{iq}^{att}} + \underbrace{\omega L_T i_{2d}}_{V_{iq}^{eq}} \quad (41)$$

Equations (40) and (41) show that V_{id}^{att} and V_{iq}^{att} include the time derivatives of S_{i2d} and S_{i2q} . The selection of a constant velocity and a proportional action attractive structure [11], allows the deduction of V_{id}^{att} and V_{iq}^{att} , which are given by the following equations

$$V_{id}^{att} = -L_T \frac{dS_{i2d}}{dt} = -L_T (-Q_d \operatorname{sgn}(S_{i2d}) - K_d S_{i2d}) \quad (42)$$

$$V_{iq}^{att} = -L_T \frac{dS_{i2q}}{dt} = -L_T (-Q_q \operatorname{sgn}(S_{i2q}) - K_d S_{i2q}) \quad (43)$$

Where Q_d , K_d , Q_q and K_q are positive constants. Based on equations (40), (41), (42) and (43), V_{id}^* and V_{iq}^* are expressed as follows

$$\begin{aligned} V_{id}^* &= V_{id}^{att} + V_{id}^{eq} \\ &= L_T (-Q_d \operatorname{sgn}(S_{i2d}) - K_d S_{i2d}) + V_{gd} - \omega_g L_T i_{2q} \end{aligned} \quad (44)$$

$$\begin{aligned} V_{iq}^* &= V_{iq}^{att} + V_{iq}^{eq} \\ &= L_T (-Q_q \operatorname{sgn}(S_{i2q}) - K_q S_{i2q}) + \omega_g L_T i_{2d} \end{aligned} \quad (45)$$

The tuning of the K ($K=K_d=K_q$) and Q ($Q=Q_d=Q_q$) constants as well as the virtual resistor K_r is detailed in the following steps.

3.2. Choice of K_r

The main goal of the VRAD method is to eliminate the real damping resistor R_d and its associated power losses. Fig.7.a and Fig.8 respectively show the un-damped and damped high frequency equivalent single phase representation of an LLCL filter without considering the grid impedance.

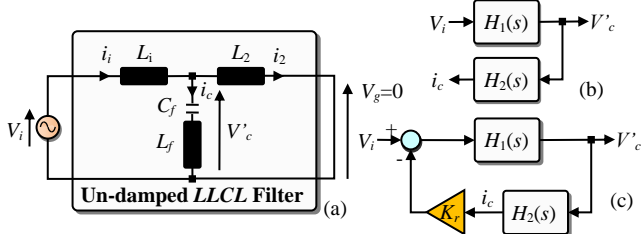


Fig. 7. High frequency single phase circuit (a) without damping resistor (b) block diagram of the LLCL filter (c) modified control structure

For the circuit given by Fig.7.a, the transfer function between

V_c' and V_i is expressed by equation (46), while the transfer function between i_c and V_c' is expressed by equation (47). Based on these equations, the un-damped high frequency LLCL filter model is given by Fig.7.b. According to Fig.5 and Fig.7.b, the control structure of the VRAD method can be presented by Fig.7.c. Based on this figure, the transfer function H_3 of the modified system is given by equation (48). When passive damping is realized by adding a resistor R_d in series with the filter capacitor (Fig.8), the transfer function G_1 of the whole system is given by equation (49). In order to obtain the same poles for the system with VRAD method and the one with a real damping resistor R_d , the denominators of H_3 and G_1 must be equal. As a result, the K_r value can be deduced according to equation (50). Thus, by considering the selected damping resistor R_d in Section 2.2 ($R_d=6\Omega$), the corresponding K_r value deduced from equation (50) is equal to 18.

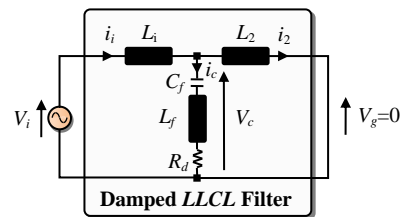


Fig. 8. High frequency single phase circuit with damping resistor in series with the filter capacitor

$$H_1 = \frac{V_c'}{V_i} = \frac{L_2(1 + C_f L_f s^2)}{C_f(L_1 L_2 + L_1 L_f + L_2 L_f)s^2 + L_1 + L_2} \quad (46)$$

$$H_2 = \frac{i_c}{V_c'} = \frac{C_f s}{1 + C_f L_f s^2} \quad (47)$$

$$H_3 = \frac{L_2(1 + C_f L_f s^2)}{C_f(L_1 L_2 + L_1 L_f + L_2 L_f)s^2 + C_f L_2 K_r s + L_1 + L_2} \quad (48)$$

$$G_1 = \frac{L_2(1 + C_f L_f s^2 + C_f R_d s)}{C_f(L_1 L_2 + L_1 L_f + L_2 L_f)s^2 + C_f R_d(L_1 + L_2)s + L_1 + L_2} \quad (49)$$

$$K_r = R_d \frac{L_1 + L_2}{L_2} \quad (50)$$

3.3. Choice of K and Q

Fig.9 and Fig.10 respectively show the harmonic attenuation rate δ and the grid current THD with regard to K and Q values. It can be noted, based on these figures, that when K and Q increase, the harmonic attenuation rate δ and the grid current THD increase. According to Fig.9, the (K, Q) couples that ensure a harmonic attenuation rate equal to 7% (value selected by the designer during the LLCL filter design) are (150,300), (200,350), (350,350), (300,250), (400,200), (400,250) and (350,100). Based on Fig.10, all the previously selected (K, Q) couples ensure a grid current THD value below than 5%. This is due to the fact that the chosen harmonic attenuation rate δ is very low (7%). For the selected (K, Q) couples, the corresponding grid current THD values are 2.2%, 3.2%, 3.9%, 2.6%, 2.2%, 2.18% and 1.3%,

respectively.

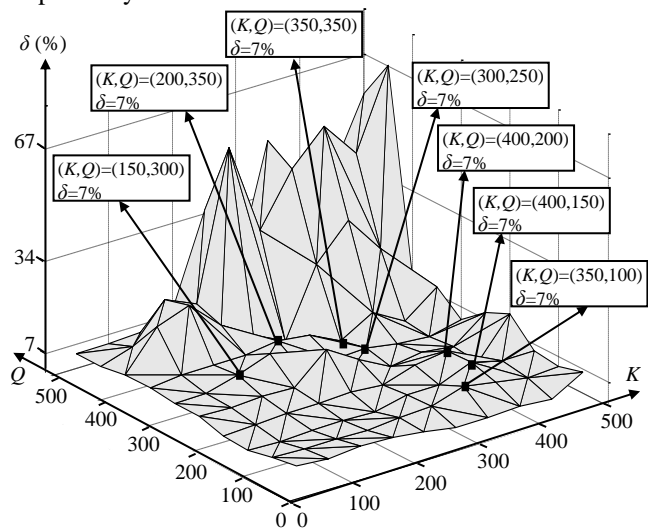


Fig. 9. Harmonic attenuation rate δ according to (K,Q)

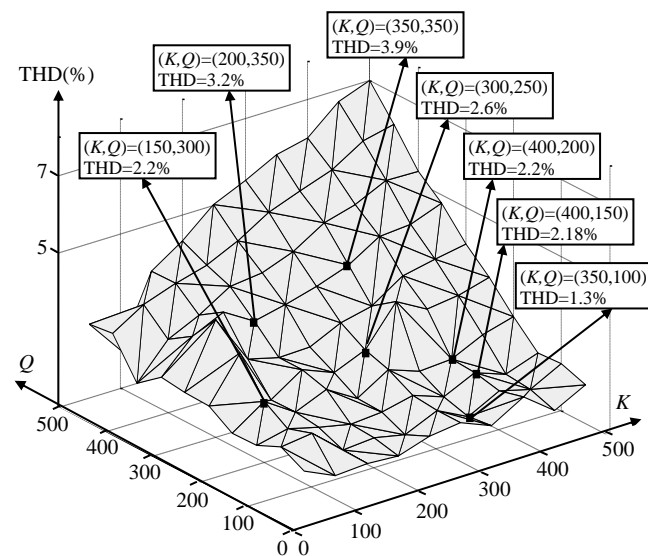


Fig. 10. Grid current THD according to (K,Q)

Fig.11 and Fig.12 respectively show the harmonic attenuation rate δ and the grid current THD value with regard to the grid impedance change for the obtained (K,Q) couples. In order to avoid system instability due to resonance problems and large grid impedance variations, δ must be between 3.3% and 34% and in order to meet new grid codes and power quality requirements, the grid current THD value must be below 5%. It can be noted, according to Fig.12, that the grid current THD is lower than 5% for the different values of (K,Q) and despite the high grid impedance variation. However, when L_g increases, the harmonic attenuation rate δ is decreased for a large set of (K,Q) couples as shown in Fig.11. The (K,Q) couples that ensure at the same time an harmonic attenuation rate δ between 3.3% and 34% and a grid current THD value lower than 5%, even for a large grid impedance variation are (350,350), (150,300) and (200,350). A value of (150,300) was chosen for the (K,Q) couple.

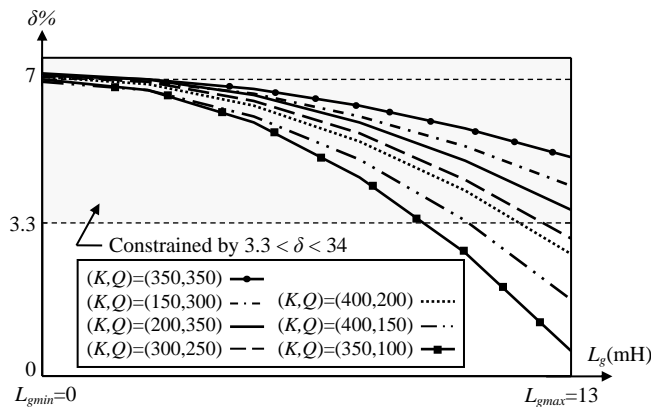


Fig. 11. Harmonic attenuation rate δ according to grid impedance L_g variation for different values of (K,Q)

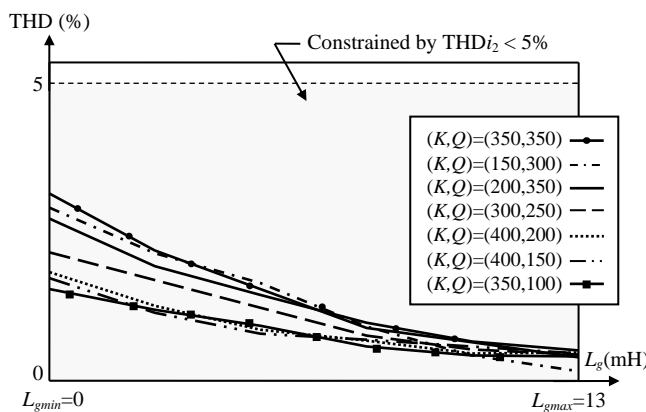


Fig. 12. Grid current THD according to grid impedance L_g variation for different values of (K,Q)

Moreover, the robustness of the system against filter parameters variations was investigated for the selected (K,Q) couple. Tab.2 shows the harmonic attenuation rate δ and the grid current THD for L_g equal to 13mH, C_f varies from 1.6 μ F to 2.4 μ F (2μ F $\pm 20\%$), L_i varies from 4mH to 6mH ($5\text{mH}\pm 20\%$), L_f varies from 50.66 μ H to 75.99 μ H (63.33μ H $\pm 20\%$) and L_2 varies from 1.6mH to 2.4mH ($2\text{mH}\pm 20\%$). It is found that for all these cases, the harmonic attenuation rate δ is larger than 3.3% and the grid current THD is below 5%. So, the system stability is ensured under large variations of grid impedance and LLCL filter parameters.

Table 2. Harmonic attenuation rate δ and grid current THD value for large grid impedance variation and LLCL filter parameters variation

$L_g=13\text{mH}$		δ (%)	THD (%)
$L_i \pm 20\%$ (mH)	4	4.3	1.4
	6	4.8	1.7
$C_f \pm 20\%$ (μ F)	1.6	3.6	0.89
	2.4	4.1	0.94
$L_f \pm 20\%$ (μ H)	50.66	3.45	0.76
	75.99	3.55	0.78
$L_2 \pm 20\%$ (mH)	1.6	3.42	0.73
	2.4	3.4	0.6

The obtained controller parameters are $K_r=18$, $K=150$ and $Q=300$. The ISMPC-VRAD algorithm was tested based on Matlab-Simulink software tool. During simulation tests, the switching frequency is equal to 10kHz and the dc-link capacitor is firstly charged to 100V. Fig.13.a and Fig.13.b present the responses of the dc-link voltage V_{dc} and the grid

current i_{2a} before and after connecting a resistive load $R_{ch}=80\Omega$ in the DC side at 0.25s. It can be noted that the V_{dc} voltage is controlled with good accuracy during steady state operation. Fig.13.c shows the waveform of the grid current i_{2a} with regard to the grid voltage V_{ga} during steady state operation.

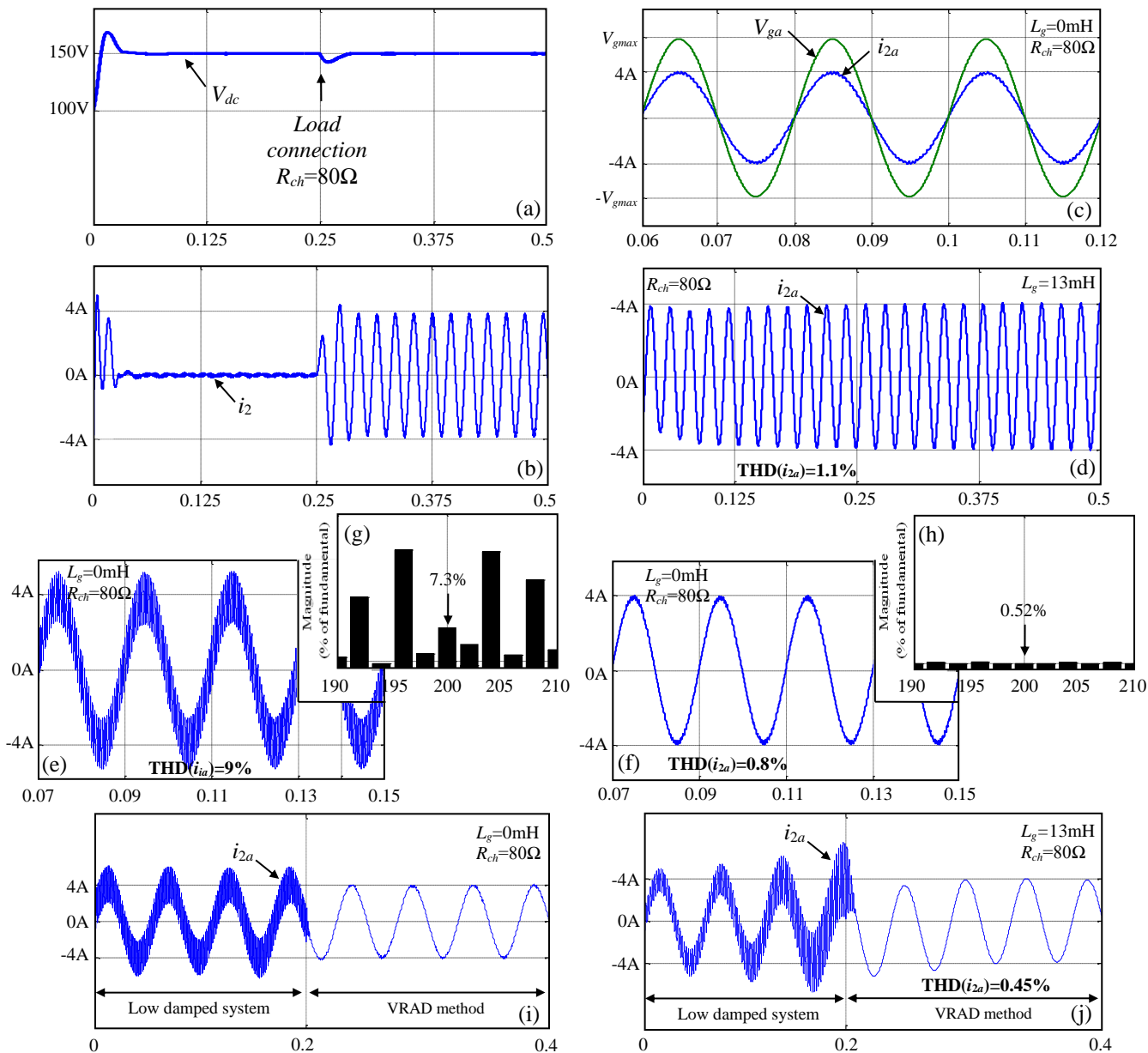


Fig. 13. (a) dc-link voltage V_{dc} response (b) grid current i_{2a} response (c) grid voltage V_{ga} and current i_{2a} waveforms at steady state operation (d) grid current i_{2a} response for $L_g=13mH$ (e) power converter current i_{ia} response (f) grid current i_{2a} response (g) high frequency spectra of i_{ia} (h) high frequency spectra of i_{2a} (i) i_{2a} before and after enabling the VRAD method at 0.2s for $L_g=0mH$ (a) i_{2a} before and after enabling the VRAD method at 0.2s for $L_g=13mH$

Based on this figure, a unit power factor operation was obtained as expected. Fig.13.e and Fig.13.f show the simulation results of the converter current i_{ia} and grid current i_{2a} , respectively. It can be noted that the current harmonic components are almost disappeared at the switching frequency. The THD of the simulated converter current is

equal to 9%, while the one of the simulated grid current is equal to 0.8%. Fig.13.g and Fig.13.h respectively present the high frequency spectra of the simulated converter and grid currents. Based on these figures, the switching frequency current harmonic component on the converter side i_{iso} is equal to 7.3% and the one on the grid side i_{2so} is equal to 0.52%.

Thus, the harmonic attenuation rate δ is well equal to 7%. In order to test the robustness of the ISMPC-VRAD, additional inductors of 13mH are inserted in series with the *LLCL* filter grid side inductor. As shown in Fig.8.d, the system remains stable despite of a large variation of the grid inductor value. Fig.13.i and Fig.13.j shows the grid current of a low damped system and the one of a damped system through VRAD method for $L_g=0\text{mH}$ and $L_g=13\text{mH}$, respectively. According to these figures, when the system is low damped, the resonance ripples are clearly increased and the system is close to the instability region. By enabling the active damping at 0.2s, the resonance ripples are damped out and the system becomes more stable despite of a large variation of the grid inductor value. Simulation results indicate the effectiveness and the robustness of both ISMPC-VRAD algorithm and the designed *LLCL-GcC*. Finally, Tab.3 shows a comparison

between the ISMPC-VRAD for *LLCL-GcC* and the VOC-VRAD for *LCL-GcC* [24]. In this comparison, the *LCL* and *LLCL* filters parameters are the same (except for *LCL* filter, the L_f value is equal to 0mH). This table shows that the ISMPC-VRAD for *LLCL-GcC* has better performances compared to the VOC-VRAD for *LCL-GcC*. This is due to the fact that the *LLCL* filter ensures higher filtering performances at the switching frequency (lower grid current THD value) compared to the *LLCL* filter thanks to the use of the additional small inductor in series with the filter capacitor. Moreover, the ISMPC-VRAD is characterized by faster transient response thanks to the non-use of integral terms, lower grid current THD value as well as more robustness against external disturbances and parameters variations compared to the VOC-VRAD.

Table 3. Comparison between performances of VOC-VRAD for *LCL-GcC* and ISMPC-VRAD for *LLCL-GcC*

Criteria/Control strategy		VOC-VRAD for <i>LCL-GcC</i>	ISMPC-VRAD for <i>LLCL-GcC</i>
Dc-link voltage regulation		++	++
Unity power factor operation		++	++
Transient response		-	++
Use of Integral terms		-	++
Tuning of control parameters		-	+
Grid current THD value ($f_{sw}=10\text{kHz}$)		1.4%	0.8%
Robustness against large variation of L_g ($f_{sw}=10\text{kHz}$ and $L_g=13\text{mH}$)	Stability	+	+++
	Grid current THD	0.7%	0.45 %
	Stability for filter parameters variation (overestimated to $\pm 20\%$)	+	++

4. Conclusion

This paper proposed an ISMPC-VRAD for the *LLCL-GcCs*. To this purpose, the *LLCL* filter design parameters as well as the ISMPC-VRAD gains have been carefully computed in order to ensure stable operation under severe grid inductance variations (overestimated to 13mH) while taking into account the influence of *LLCL* filter parameters changes (overestimated to $\pm 20\%$) on the system stability. The obtained simulation results gave proof of the effectiveness, performances and reliability of the implemented ISMPC-VRAD algorithm as well as the high filtering performances of the used *LLCL-GcCs*.

Acknowledgements

“This work was supported by the Tunisian Ministry of High Education and Research under Grant LSE-ENIT-LR11ES15”

References

- [1] M.A. Elsharty, H.A. Ashour. Passive L and LCL Filter Design Method for Grid-Connected Inverters, *IEEE Conference in innovative Smart grid technologies*, pp.13-18, 2014.
- [2] S. Jayalath, M. Hanif, “Generalized LCL-Filter Design Algorithm for Grid-connected Voltage Source Inverter”, *IEEE Trans. Ind. Electron*, vol. PP, pp.1537–1547, 2016.
- [3] S. Lim, J. Choi et al., “LCL Filter Design for Grid Connected NPC Type Three-Level Inverter”, *International Journal of Renewable Energy Research*, vol. 5, pp. 45-53, 2015.
- [4] J. Fang, H. Li, Y. Tang, “A magnetic Integrated LLCL Filter for Grid-Connected Voltage-Source Converters”, *IEEE Trans. Power Electron*, vol. 32, pp. 1725-1730, 2017.
- [5] M. Sanatkar-Chayjani, M. Monfared, “Design of LCL and LLCL filters for single-phase grid connected converters”, *IET Power Electron.*, vol. 9, pp.1971-1978, 2016.
- [6] M. Huang, X. Wang, P. Chiang Loh, F. Blaabjerg, “Design of the LC + Trap filter for a current source rectifier”, *European Conference on Electronics and Applications and Applications*, pp. 1-9, 2015.
- [7] J. M. Bloemink, T C. Green, “Reducing Passive Filter Sizes with Tuned Traps for Distribution Level Power Electronics”, *IEEE EPE*, pp.1-9, 2011.
- [8] J. Dannehl, F.W. Fuchs, P.B. Thogersen, “PI Space Current Control of Grid-Connected PWM Converters with LCL Filters”, *IEEE Trans. Power Electron.*, vol. 25, pp.2320-2330, 2010.
- [9] R. Teodorescu, M. Liserre, P. Rodriguez, Grid Filter Design. *Wiley-IEEE Press eBook Chapters*, 2011, 289-

- 312.
- [10] M. Malinowski, M. Jasinski, M. P. Kazmierkowski, "Simple direct power control of three-phase PWM rectifier using space-vector modulation (DPC-SVM)", *IEEE Trans. Indus. Electron.*, vol.51, pp.447-454, 2004.
- [11] A. Hemdani, M. Dagbagi, M.W. Naouar, L. Idkhajine, I. Slama-Belkhdja, E. Monmasson, "Indirect sliding mode power control for three phase grid connected power converter", *IET Power Electron.*, vol.8, pp.977-985, 2015.
- [12] A. Djerioui, K. Aliouane, F. Bouchafaa, "Sliding Mode Observer of a Power Quality in Grid Connected Renewable Energy Systems", *International Journal of Renewable Energy Research*, vol. 2, pp. 541-548, 2012.
- [13] R. N. Beres, X. Wang, F. Blaabjerg, M. Liserre, C. L. Bak, "Optimal Design of High-Order Passive-Damped Filters for Grid-Connected Applications", *IEEE Trans. Power Electron*, vol. 31, pp.2083-2098, 2016.
- [14] M. Buyuk, A. Tan, M. Tumay, K. Cagatay Bayindir, "Topologies, generalized design, passive and active damping methods of switching ripple filters for voltage source inverter; A comparative review", *Renew Sustain Energy Rev.*, vol. 62, pp. 46-49, 2016.
- [15] M. Huang, X. Wang, P. C. Loh, F. Blaabjerg, "Active Damping of LLCL-Filtered Resonance Based on Lc-Trap Voltage or Current Feedback", *IEEE Trans. Electron.*, vol. 31, pp.2337-2346, 2016.
- [16] W. Yao, Y. Yang, X. Zhang, F. Blaabjerg, P. Loh, "Design and Analysis of Robust Active Damping for LCL Filters using Digital Notch Filters", *IEEE Trans Power Electron.*, vol. 32, pp.2360-2375, 2017.
- [17] R. Peña-Alzola, M. Liserre, F. Blaabjerg, R. Sebastian, F.W. Fuchs, "Systematic Design of the Lead-Lag Network Method for Active Damping in LCL-Filter Based Three Phase Converters", *IEEE Trans. Indus. Inform.*, vol. 10, pp. 43-52, 2014.
- [18] K. Park, F. Kieferndorf, U. Drogenik, S. Pettersson, F. Canales, "Weight Minimization of LCL Filters for High Power Converters", *IEEE Transaction on Industry Applications*, vol. PP, pp.1-1, 2017.
- [19] Z. Xin, P. Ching, X. Wang, F. Blaabjerg, Y. Tang, "Highly accurate derivatives for LCL-filtered grid converter with capacitor voltage active damping", *IEEE Tran. Power Electron*, vol.31, pp.3612-3625, 2016.
- [20] X. Li, X. Wu, Y. Geng, X. Yuan, C. Xia, X. Zhang, "Wide Damping Region for LCL-Type Grid-Connected Inverter With an Improved Capacitor-Current-Feedback Method", *IEEE Trans. Power Electron.*, vol. 30, pp. 5247-259, 2015.
- [21] K. Koiwa, M. Rosyadi, A. Umemura, R. Takahashi, J. Tamura, "Sensorless virtual resistance damping method for grid-connected three-phase PWM converter with LCL filter", *International conference on Electrical Machines and Systems*, pp. 1746-1749, 2013.
- [22] C. Bae, P. Alemi, D. Lee, "Resonance elimination of LLCL filters based on virtual resistor for single-phase PWM inverters", *International Conference on Power Electronics and ECCE Asia*, pp. 2875-2880, 2015.
- [23] E. Chaves, E. Coelho, H. Carvalho, L. Freitas, J. Junior, L. Freitas, "Design of an Internal Model Control strategy for single-phase grid-connected PWM inverters and its performance analysis with non-linear local load and weak grid", *ISA Trans.*, vol. 64, pp. 373-383, 2016.
- [24] M. Ben Saïd-Romdhane, M.W Naouar, I. Slama-Belkhdja, E. Monmasson, "Robust Active Damping Methods for LCL Filter Based Grid Connected Converters", *IEEE Trans. Electron.*, vol. PP, pp.1-1, 2016.
- [25] J. He, Y. Wei Li, D. Xu, X. Liang, B. Liang, C. Wang, "Deadbeat Weighted Average Current Control With Corrective Feed-Forward Compensation for Microgrid Converters with Nonstandard LCL Filter", *IEEE Trans. Electron.*, vol. 32, pp.2661-2674, 2017.
- [26] J. Fang, X. Li, X. Yang, Y. Tang, "An Integrated Trap-LCL Filter with Reduced Current Harmonics for Grid-Connected Converters under Weak Grid Conditions", *IEEE Trans. Electron.*, vol. PP, pp.1-1, 2017.
- [27] M. Ben Saïd-Romdhane, M.W. Naouar, I. Slama-Belkhdja, E. Monmasson, "Simple and systematic LCL filter design for three-phase grid-connected power converters", *Math. Computers Simul.*, vol. 130, pp.181-193, 2016.
- [28] IEEE Standard 519-1992, Recommended practices and requirements for harmonic control in electrical power systems, *The Institute of Electrical and Electronics Engineers*, 1993.